Materials Today Chemistry 38 (2024) 102100

Contents lists available at ScienceDirect

Materials Today Chemistry

journal homepage: www.journals.elsevier.com/materials-today-chemistry/

A simple swell-and-click method for the covalent attachment of virus-like particles to polymer hydrogels

Jorge Leganés Bayon [a,d,e], Calvin Shih [a,d,e], Stephen L. Craig [f], Nicole F. Steinmetz [a,b,c,d,e,g,h,i,*]

[a] Department of NanoEngineering, University of California San Diego, 9500 Gilman Dr., La Jolla, CA, 92093, United States
[b] Department of Bioengineering, University of California San Diego, 9500 Gilman Dr., La Jolla, CA, 92093, United States
[c] Department of Radiology, University of California San Diego, 9500 Gilman Dr., La Jolla, CA, 92093, United States
[d] Center for Nano-ImmunoEngineering, University of California San Diego, 9500 Gilman Dr., La Jolla, CA, 92093, United States
[e] Shu and K.C. Chien and Peter Farrell Collaboratory, University of California San Diego, 9500 Gilman Dr., La Jolla, CA, 92093, United States
[f] Department of Chemistry, Duke University, Durham, NC, 27708, United States
[g] Center for Engineering in Cancer, Institute of Engineering in Medicine, University of California San Diego, 9500 Gilman Dr., La Jolla, CA, 92093, United States
[h] Moores Cancer Center, University of California, University of California San Diego, 9500 Gilman Dr., La Jolla, CA, 92093, United States
[i] Institute for Materials Discovery and Design, University of California San Diego, 9500 Gilman Dr., La Jolla, CA, 92093, United States

ARTICLE INFO

Keywords:
Virus-like particle
Hydrogel
Swelling
Click, release

ABSTRACT

Plant virus-like particles (VLPs) are biocompatible, non-infectious nanomaterials with promising applications as immunotherapeutics and vaccines. However, slow-release VLP formulations are needed to achieve long-term efficacy without repeated administration. VLP hydrogels allow the encapsulation and sustained delivery of VLPs, but the particles must covalently bind the hydrogel polymers to avoid premature loss. This has been achieved so far by *in situ* VLP polymerization, which requires high viral concentrations (5–10 mg/mL, 0.5–1 wt %) to form stable hybrid VLP–hydrogel networks and this complicates scalability and clinical translation. Here, we developed a novel swell-and-click method that led to successful VLP scaffold formation regardless of the viral load used. As a result, VLP-functionalized hydrogels were fabricated with viral concentrations as low as 0.1–1 mg/mL (0.01–0.1 % wt%) without compromising the scaffold stability on the process. The hydrogels incorporate VLPs during swelling, followed by copper-free click chemistry reactions that bind the particles covalently to the polymer. The swell-and-click method also resulted in more than a two-fold enhancement in VLP uptake into the hydrogels and it provides a means of combined burst release and prolonged sustained release, desired traits for cancer immunotherapy treatment. The present work introduces a novel methodology for the design of VLP-based hydrogels, which could facilitate the scalability of the fabrication process and move a significant step forward towards clinical translation of long-term VLP vaccination in cancer disease.

1. Introduction

Plant virus-like particles (VLPs) are protein-based nanomaterials with a highly defined 3D structure, often icosahedral or tubular, that can be produced in the laboratory with yields of tens or hundreds of milligrams [1]. These nanoparticles are highly biocompatible, biodegradable and non-infectious, allowing them to be repurposed for applications such as drug delivery, cancer vaccines, and immunotherapy [2]. For example, intratumoral immunotherapy based on plant VLPs has been used to treat canine cancer patients [3]. Nevertheless, when used as immunotherapy for chronic diseases or cancer vaccines [4], repeated and even life-long dosing may be required [5]. VLP depots that facilitate slow release over time would avoid this need for repeat administration [5].

Hydrogels are 3D crosslinked polymer networks that form outstanding slow-release formulations due to their physical mimicry of tissues (70–99 % water content) and their unique porous and highly tunable architecture [6,7]. Polymer hydrogels accommodate a variety of bioactive compounds [8–10], and controlled-release formulations can be used to extend the therapeutic window [11,12]. Some studies have explored the incorporation of virus nanoparticles (VNPs, which unlike VLPs retain the viral genome) into hydrogels as fillers to enhance mechanical performance or tissue engineering [13]. Others have developed hydrogels for the slow release of VLPs or therapeutic molecules,

* Corresponding author. Department of NanoEngineering, University of California San Diego, 9500 Gilman Dr., La Jolla, CA, 92093, United States.
E-mail address: nsteinmetz@ucsd.edu (N.F. Steinmetz).

https://doi.org/10.1016/j.mtchem.2024.102100
Received 8 April 2024; Received in revised form 7 May 2024; Accepted 10 May 2024
Available online 3 June 2024

including cowpea chlorotic mottle virus (CCMV)–chitosan supramolecular hydrogels that reduced the initial burst release of VLPs by controlling host–guest interactions [14], and tobacco mosaic virus (TMV) and bacteriophage M13 particles modified with β-cyclodextrin to form a host–guest crosslinked hyaluronan hydrogel that controlled cell release during the sol–gel transition [15]. Furthermore, cowpea mosaic virus (CPMV) particles have been entrapped in chitosan hydrogels that released the viral cargo for several weeks to prolong immunostimulation *in vivo* [16].

These examples show that VLPs can be trapped in hydrogels for slow release, but covalent bonds between the VLPs and the hydrogel scaffold are necessary for long-term release profiles. The covalent integration of VLPs into polymer networks is a largely underexplored area, highlighting the unique challenges of VLPs as high-molecular-weight (MDa) biologics with a high degree of multivalency, the latter allowing their use as high-avidity multifunctional crosslinkers. One such platform is TMV, a rod-like virus consisting of 2130 identical coat protein subunits each with a cross-linkable tyrosine residue (Tyr139) [17]. The ability to crosslink TMV has been explored comprehensively, resulting in the diazonium coupling of surface-exposed tyrosines to covalently crosslink TMV into a hydrogel network with viral concentrations as low as 2.5 mg/mL (0.25 wt%) while still allowing gelation [18]. However, such hydrogel formulations suffer from poor structural stability, as demonstrated by a simple test tube inversion [19]. Similar sol-like hydrogels were combined with copper-free *click* chemistry to covalently crosslink alkyne-modified CCMV into a mechanically responsive hydrogel [20]. The covalent incorporation of VNPs into structurally consistent hydrogels has been achieved by copolymerizing the cysteine TMV mutant (TMV-cys) with PEGDA crosslinkers under UV light, resulting in well-defined TMV-crosslinked solid hydrogels [21]. However, high concentrations of PEGDA (200 mg/mL, 20 wt%) and TMV-cys (10–20 mg/mL, 1–2 wt%) were required to achieve sufficient covalent crosslinking of the VNP to the already densely crosslinked PEGDA network. Because proteins are known to undergo disulfide cleavage as well as radical transfer when exposed to UV radiation, this approach could also lead to VLP aggregation [22].

All studies reported thus far have focused on incorporating the VLP covalently into a hydrogel *via in situ* polymerization, wherein a polymer (and/or a chemical crosslinker agent, such as PEGDA) is mixed along with the VLP crosslinker in solution to polymerize the hydrogel *in situ*. This approach has the inherent disadvantage that the successful formation of a stable hydrogel with a covalently integrated VLP cargo will always require high concentrations of VLP crosslinker in the polymerization medium (5–20 mg/mL, 0.5–2 wt%), which makes the process less scalable. Even if the material is fabricated successfully, crosslinking the VLP during polymer synthesis will alter the mechanical fate of the hydrogel, which makes it difficult to control independently the VLP loading and hydrogel properties such as stiffness, hydrophilicity and microstructure [23]. This limits the adjustment of the VLP cargo to match a given therapeutic window, which is necessary for clinical translation.

To overcome these technological challenges, we developed a novel method for the covalent functionalization of hydrogels with VLPs without relying on viral concentration to achieve successful gelation. VLP concentrations as low as 0.1–1 mg/mL (0.01–0.1 wt%) were used to fabricate VLP-based hydrogels with excellent mechanical stability. The hydrogels were chemically crosslinked to ensure mechanical stability and integrity in the absence of VLPs, which were incorporated using a post-synthesis *swell-and-click* approach. Solutions of alkyne-functionalized VLPs were added to dehydrated xerogels of azide-functionalized polymer networks, and the VLPs were efficiently taken up into the polymer network during the xerogel-to-hydrogel transition due to the swellability of the xerogels. The alkyne-functionalized VLPs then underwent copper-free *click* chemistry with the polymer to form robust covalent bonds even at very low VLP concentrations. The hydrogels retained the covalently attached VLPs, which lead to a combined partial premature particle release followed by sustained release in vitro over a period of several months. The novel materials could be used for the development of extended controlled-release formulations, such as single-dose VLP implants to tackle chronic diseases where repeated administration is typically required.

2. Materials and methods

2.1. Expression and preparation of PhMV-VLPs

BL21 glycerol stocks containing pRSETa-PhMV CP and pET-PhMV CP previously reported [24] were inoculated into 50 mL of Lysogeny Broth (LB) containing 50 μg/mL of carbenicillin and 50 μg/ml kanamycin and the culture was incubated for 18 h (37 °C, 225 rpm). 10 mL of the preculture were then inoculated into 500 mL of Terrific Broth (TB) also containing carbenicillin and kanamycin 50 μg/ml and allowed to incubate (37 °C, 250 rpm). When culture density reached an OD_{600}~1 (approximately 8 h), protein expression was induced with 0.5 mM isopropyl-β-D-1-thiogalactopyranoside (IPTG; Gold Biotechnology), and the cells were incubated overnight (30 °C, 250 rpm). The culture was then centrifuged (7500×*g*, 10 min, 4 °C), the cell pellet was resuspended in 50 mM sodium citrate buffer (SCB) and the resulting suspension was sonicated (10 min, 30 % amplitude, 5 s ON, 2 s OFF) and centrifuged (10,000×*g*, 10 min, 4 °C). The supernatant was collected and centrifuged (27,000×*g*, 30 min, 4 °C). The supernatant was then subjected to ultracentrifugation (35,000 rpm, 3 h, 4 °C, 50.2 Ti rotor, Beckman Coulter). The resulting pellets were resuspended in SCB overnight. Insoluble material was removed by centrifugation (15,000×*g*, 10 min, 4 °C). Supernatant was extracted with 1:1 $CHCl_3$/BuOH and the aqueous layer was isolated by centrifugation (5000×*g*, 10 min, 4 °C). The resulting solution was centrifuged (15,000×*g*, 10 min, 4 °C) to remove insoluble material. The suspension was then layered carefully onto a 10−40 % (w/v) linear sucrose gradient and ultracentrifuged (28,000 rpm, 3 h, 4 °C, SW32 rotor, Beckman Coulter). The light scattering fractions were pooled, diluted in SCB 1:1, and concentrated by ultra-centrifugation (42,000 rpm, 3 h, 4 °C, 50.2 Ti rotor, Beckman Coulter). The clear colorless pellet was finally resuspended in PBS pH 7.2 and stored at 4 °C. The VLP concentration was measured using a bicinchoninic acid (BCA) assay using bovine serum albumin (BSA) as a standard.

2.2. Bioconjugation of PhMV VLPs

General protocol: To a VLP solution in PBS (5 mg/mL), the corresponding bioconjugate reactant was added overnight at room temperature, followed by concentration with ultracentrifugation (52,000 rpm, 70 min, 4 °C, TLA 55 rotor, Beckman Coulter) over a 100 μL sucrose cushion (20 % sucrose in PBS). The pellet was washed, resuspended, and centrifuged at 15.000×*g* for 10 min and the supernatant collected.

PhMV-cy5.5: sulfo-Cyanine5.5 maleimide (5 eq/CP, Lumiprobe) was added to target inner cysteines (C75). Yields: 45 %. *PhMV-yne:* sulfo dibenzocyclooctyne (DBCO)-PEG3-NHS ester (10 eq/CP, BroadPharm) and sulfo-Cyanine5.5 maleimide (5 eq/CP, Lumiprobe) were added one-pot to target external lysines (K62, K143, K153, and K166) and internal cysteines, respectively. Yields: 55 %. *PhMV-DBCO:* sulfo-DBCO-PEG3-NHS ester (10 eq/CP, BroadPharm) was added to target external lysines. *PhMV-(C)lick*: AC-PEG2K–N_3 (120, 600, and 1200 eq/CP, Creative PEGworks) was added to PhMV-DBCO solution in PBS (1 mg/mL) following a strain-promoted azide-alkyne cycloaddition (SPAAC).

2.3. Characterization of PhMV VLPs

Size Exclusion Chromatography (SEC) was carried out using a Superose-6 Increase 10/300 GL column ($P_i = 5$ MPa, $\Delta P = 5$ MPa) on the Äkta Pure system (Cytiva). The column was loaded with 250 μL sample (1.4 mg/mL) and the sample was run for 50 min at a flow rate of 0.5 mL/

min in PBS buffer. Denatured protein subunits (5 μ) were analyzed by polyacrylamide gels electrophoresis using 12 % NuPAGE gels and 1 × MOPS buffer (Invitrogen). Samples were denatured by boiling in 1:10 reducing agent and 1:4 SDS blue loading dye for 5 min. Intact PhMV VLPs (5 μg) were analyzed using 0.8 % (w/v) native agarose gel electrophoresis in 0.1 M Tris-borate-EDTA (TBE) running buffer (pH 8.3). All gels were stained in Coomasie blue staining followed by photography under UV or far-red light in a FluorChem R system (Bio-Techne). Dynamic light scattering (DLS) analysis was performed in a Zetasizer Nano ZSP/Zen5600 instrument (Malvern Panalytical, Malvern, UK). All VLP samples were measured at a concentration of 0.4 mg/mL in PBS. Transmission electron microscopy (TEM) analysis was performed using a JEOL 1400 plus high-resolution EM operating at 80 kV and equipped with a bottom-mount Gatan OneView (4 k x 4 k) camera. For imaging, samples were prepared by dip-casting VLP solutions (1 mg/mL) onto carbon-coated grids (Electron Microscopy Sciences) and washed with DI water (3×) prior to staining with 2 % (w/v) uranyl acetate.

2.4. Synthesis of hydrogels (HGs) and VLP hydrogels (VHGs)

All reagents were purchased from Aldrich except otherwise stated. Hydrogels (HGs) were synthesized *via* free radical photopolymerization as follows: Polyethylene glycol methacrylate MW = 480 Da (PEGMA, 200 mg/mL, 417 mM), acrylamide (AAm, 150 mg/mL, 2110 mM), polyethylene glycol diacrylate MW = 700 Da (PEGDA, 2.5 mg/mL, 3.6 mM) and lithium aryl phospinate (LAP, 5 mg/mL, 17 mM) were dissolved in PBS followed by addition of Acrylate-PEG2K-azide MW = 2000 Da (AC-PEG2K–N_3, 100 mg/mL, 48.3 mM, Creative PEG works) in PBS. 300 μL of yellowish mix were then casted into disk-shaped PDMS molds (8 mm diameter x 3 mm height, SYLGARD®184 kit) and cured for 10 min (λ = 254 nm, 120,000 μJ/cm^2) in a UV reactor (CL-1000 254 UV crosslinker, UVP). HGs were then washed in MilliQ water, which was replenished (twice a day, four days), and dried gently at 30 °C until full dryness (xerogel). VLP-laden hydrogels (VHGs) were then designed following a *swell-and-click* approach. Namely, 300 μL PhMV-cy5.5 or PhMV-yne VLP solutions in PBS (1 mg/mL, 0.1 wt%) were added onto fully dried HG samples (~80 mg) in a sealed vial until full swelling uptake. After equilibration, the VHGs were gently dried to remove remnant water. Two xerogels were this way prepared, VLP-native hydrogel (VN-HG) and VLP-*clicked* hydrogel (VC-HG) from the PhMV-cy5.5 and PhMV-yne solutions, respectively.

2.5. Characterization of hydrogels (HGs) and VLP hydrogels (VHGs)

Thermogravimetric analysis (TGA) was performed by analyzing sliced xerogel samples (25–40 mg), lyophilized VLPs (1.5–4 mg) or solid monomer powders (5–30 mg) on a Discovery SDT 650™ (TA Instruments™) simultaneous DSC/TGA. Samples were equilibrated at 50 °C, then ramped up at 10 °C/min until 1200 °C under N_2 atmosphere. Mechanical properties of the materials were measured in a TA Instruments™ Discovery™ HR-30 Hybrid Rheometer. Fully dried xerogels were swollen with 100 μL PBS to obtain disk samples of 9 mm diameter x 3 mm height after equilibration. Samples were then measured both for axial and frequency sweep tests. For axial compressive tests (ω = 0 rad/s), samples were compressed with a stainless-steel geometry (8.0 mm parallel plate ETC stainless steel) at an axial force of 0.3 N, gap speed of 100 μm/s and 75 % initial strain. For frequency sweep studies, the same conditions were followed, however angular velocity was set to ω = 1–250 rad/s. For both sets of experiments, 5 consecutive cycles were performed. Swelling degree (SD) studies were performed using a gravimetric method. Dried xerogel samples (~95 mg) were immersed in ultrapure water, then placed on filter paper to blot excess water and weighted at defined time intervals. The SD was calculated according to the formula: $SD = [(W_T\text{-}W_0)/W_0]$*100, where W_T and W_0 are the weights of the swollen hydrogel at time T and at time T = 0, respectively. The porosity of the hydrogels was investigated using a Zeiss Sigma 500 scanning electron microscope (SEM) operated at 3 kV accelerating voltage with a SE2 Everhart Thornley and EDS 80 mm^2 Oxford detector. Fully swollen hydrogels were freeze-dried and sliced prior to introduction in the vacuum chamber. Fourier transform infrared (FTIR) of xerogel samples (70–100 mg) was carried out in a Nicolet™ iS50 and 6700 spectrometer, fitted with Smart-iTR™ diamond Attenuated Total Reflectance (ATR) at a range of 500–4000 cm^{-1}. Samples for each technique were measured in triplicate.

2.6. VLP loading and In vitro VLP release studies

VLP loading and release readings were quantified through UV/Vis absorbance spectroscopy using an Infinite® M Plex, multimode microplate reader. Cy5.5-labeled PhMV VLPs were measured at λ_{max} = 675 nm followed by absorbance interpolation in freshly prepared calibration curves. For the loading studies: dried HG xerogels (W_0 = 70–100 mg, SD_{max}=0 wt%) were immersed in 4.95 mL PhMV-cy5.5 or PhMV-yne solutions in PBS at initial concentrations (C_i) of C_i = 0.1, 0.5 and 0.75 mg/mL (0.01, 0.05 and 0.075 wt%, respectively) for 5 days until VHGs reached maximum swelling (W_0 = 1500–2200 mg, SD_{max}=1950–2500 % wt%). The amount of loaded VLPs in the VHGs was then determined through UV/VIS detection as the amount not recovered in the PhMV-yne and PhMV-c5.5 loading solutions after hydrogel loading. Namely, *VLP loading (%)* = $[(M_t\text{-}M_u)/M_t]$*100 where M_t and M_u are the total VLP added masses and the unloaded VLP masses in the loading media. For in vitro VLP release: HG xerogels (W_0 = 70–100 mg, SD_{max}=0 wt%) were immersed in 4.95 mL PhMV-cy5.5 or PhMV-yne solutions in PBS at C_i = 0.75 mg/mL until maximum swelling (W_0 = 1950–1990 mg, SD_{max}=1950–1980 wt%The fully loaded VHGs were then immersed in 15 mL PBS and incubated at 125 rpm for two weeks at room temperature and several months at 4 °C. The cumulative release of VLPs from the VHGs was determined through UV/VIS detection of small aliquots (330 μL) at different timepoints, before pipetting back to the release medium. Namely, cumulative VLP release (%) = $[(M_R/(M_t\text{-}M_u)]$*100 where M_R, M_t, and M_u are the released VLP mass at each timepoint, the total VLP added masses and the unloaded VLP masses in the loading media, respectively.

3. Results and discussion

3.1. Synthesis and characterization of PhMV VLPs

Physalis mottle virus (PhMV) was chosen as a model VLP. PhMV is a ~30 nm icosahedral plant virus with T = 3 symmetry, comprising 180 identical ~20 kDa coat protein (CP) subunits [25]. Homogeneous and monodisperse PhMV VLPs were obtained by CP expression in bacteria [24]. We chose *click* chemistry for the covalent attachment of VLPs to hydrogels because this reaction is widely used for protein bioconjugation due to its efficiency, selectivity, and bio-orthogonality [26]. Although copper-based *click* chemistry is suitable for VLPs [27], it depends on specific pH and catalytic conditions [28]. Therefore, we used strain-promoted azide alkyne cycloaddition (SPAAC) as a simpler, catalyst-free *click* alternative. We functionalized the VLPs with a ring-strained dibenzo-cyclooctyne (DBCO) group for that purpose. We also conjugated the VLPs to a cyanine dye, allowing quantification during hydrogel loading and release. This dual modification was carried out in a one-pot process targeting different sites with spatial control (Fig. 1A). Specifically, sulfo-cyanine5.5 maleimide and DBCO-PEG3-NHS ester were added to the VLP solution to target internal cysteines (C75) and surface-exposed lysines (K62, K143, K153 and K166), respectively [29]. The resulting alkynylated, cy5.5-labeled particle was named PhMV-yne. We also synthesized an alkyne-free, cy5.5-labeled VLP as a comparative control, which was named PhMV-cy5.5. Both particles were produced with a yield of 45–55 %.

Successful functionalization and particle integrity were demonstrated using a combination of techniques. Denaturing electrophoresis

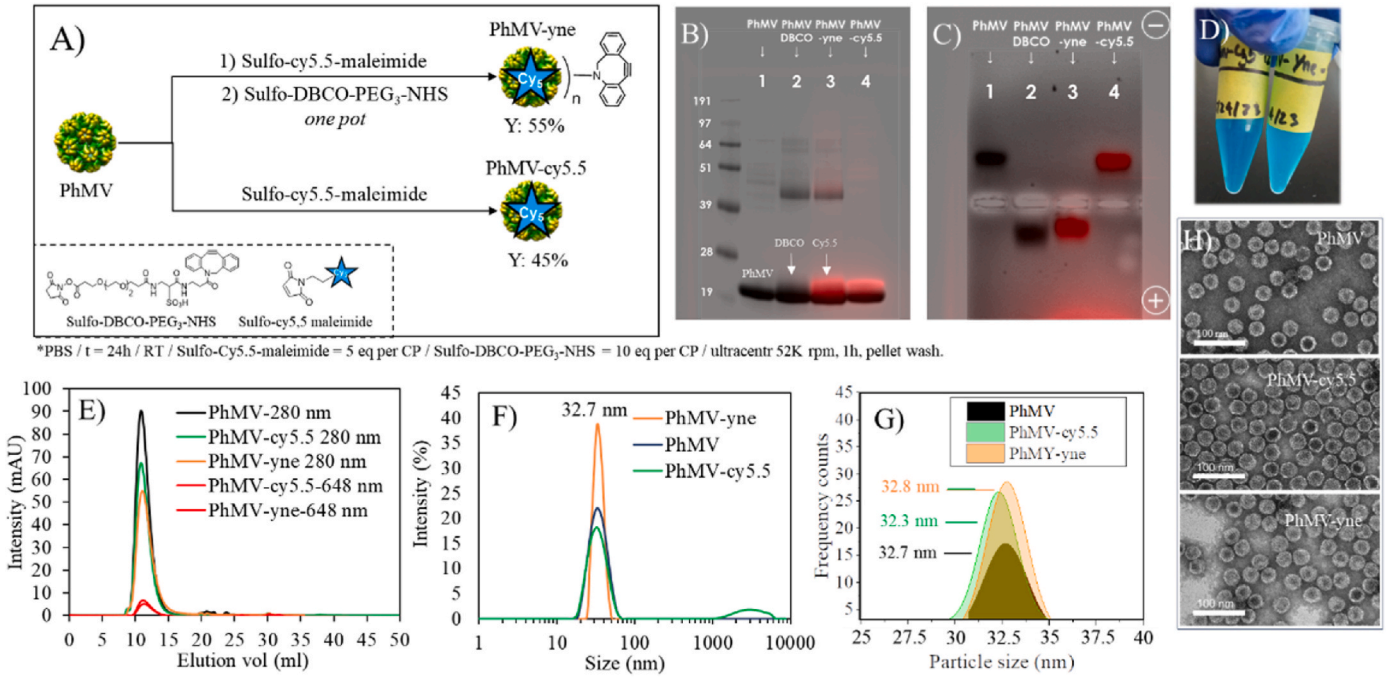

Fig. 1. Synthesis and characterization of VLPs. A) Strategy for the synthesis of VLPs. Analysis of VLPs by B) SDS-PAGE and C) native gel electrophoresis under white light, stained with Coomasie Brilliant Blue and superimposed with red fluorescence. D) Photograph of VLP solutions: PhMV-cy5.5 (left) and PhMV-yne (right). Distribution of VLP particle size as determined by E) size exclusion chromatography, F) dynamic light scattering, and G) transmission electron microscopy (TEM). H) TEM images of negatively stained VLPs. (For interpretation of the references to color in this figure legend, the reader is referred to the Web version of this article.)

(Fig. 1B) revealed the characteristic native CP band in PhMV (**1**) at ~20 kDa. Functionalization of the VLP with sulfo-DBCO-PEG$_3$-NHS (**2**) resulted in a slightly higher molecular weight, shown as smearing above the CP band. Clear separation does not occur due to the low molecular weight of the linker (756.8 Da). The presence of fluorescent bands when gels were imaged under red light confirmed cy5.5 conjugation, which was quantified by UV/vis spectrophotometry. PhMV-yne (**3**) displayed 50–55 cy5.5 dye molecules per VLP (29 % total) and PhMV-cy5.5 (**4**) displayed 70–75 per VLP (41 % total). Native electrophoresis also confirmed the bioconjugation of VLPs according to changes in particle mobility or fluorescence (Fig. 1C). Positively charged PhMV [30] (**1**) migrates toward the cathode (−), whereas functionalization with sulfo-DBCO-PEG$_3$-NHS (**2**) creates a negative charge and causes migration toward the anode (+). This is typically observed when PhMV surface lysines are neutralized during NHS ester conjugation [31]. Conversely, cy5.5 labeling was confirmed by the presence of fluorescent bands in the PhMV-yne (**3**) and PhMV-cy5.5 (**4**) lanes, with the former also shifting mobility due to the successful alkynylation of lysines with DBCO. Both VLP solutions appeared bright blue due to dye labeling (Fig. 1D). Size exclusion chromatography showed identical elution volumes for all VLPs, confirming similar particle sizes (Fig. 1C). The hydrodynamic radius was 32–33 nm as determined by dynamic light scattering (DLS)

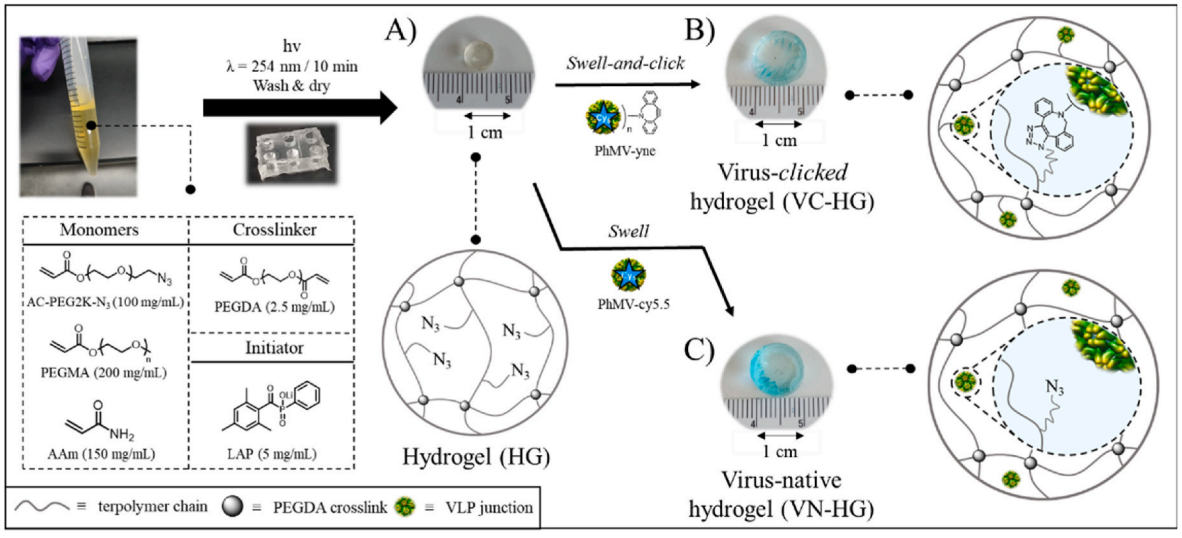

Fig. 2. *Swell-and-click* synthesis of the VLP-laden hydrogels (VHGs). Before adding VLPs, the monomers, crosslinker and initiator were photopolymerized, washed and dried, to produce A) the control hydrogel (HG). The latter was swollen in a PhMV-yne solution (*swell-and-click)* to produce B) the VLP-*clicked* hydrogel (VC-HG). In parallel, the hydrogel was swollen in a PhMV-cy5.5 solution to produce C) the VLP-native hydrogel (VN-HG). For simplicity, the polymer backbone and crosslinker are depicted as chains and round junctions, respectively.

and transmission electron microscopy (TEM) (Fig. 1F and G). DLS showed that the VLPs were monodisperse and homogeneous, and TEM imaging confirmed their uniform and icosahedral structure (Fig. 1H).

3.2. Synthesis of control hydrogels and VLP-laden hydrogels

The control hydrogel (HG) was synthesized by free-radical photopolymerization (Fig. 2). Briefly, acrylate-PEG2K-azide (AC-PEG2K–N_3), polyethylene glycol methacrylate (PEGMA), acrylamide (AAm) and polyethylene glycol diacrylate (PEGDA), were dissolved with the photoinitiator lithium arylphosphonate. The yellow viscous mix was then cast into disk-shaped PDMS molds and cured in a UV reactor for 10 min. The resulting hydrogels (Fig. 2A) were washed in water for 4 days, with water replenished twice per day, to remove unreacted components and then gently dried to form HG xerogels consisting of a terpolymer network crosslinked with PEGDA and featuring pendant azide groups (Fig. 2).

The VLP-laden hydrogels (VHGs) were then synthesized using the *swell-and-click* method. A fully dried HG xerogel was swollen in a PhMV-yne solution (300 μL, 1 mg/mL, 0.1 wt%) until all the liquid had been taken up. During swelling, the alkynylated VLP underwent SPAAC with the azide pendant groups, producing a VLP-*clicked* hydrogel (VC-HG) in which the VLP was bound covalently to the polymer backbone of the HG (Fig. 2B). The VC-HG was then carefully dried to restore the xerogel state. As a comparative VHG control, an HG xerogel was also swollen in a PhMV-cy5.5 solution (300 μL, 1 mg/mL, 0.1 wt%) producing a VLP-native hydrogel (VN-HG, Fig. 2C) that was subsequently dried to give the corresponding xerogel in which the VLP is not covalently bonded to the HG scaffold.

To the best of our knowledge, chemical reactions between VLPs and a swelling hydrogel have not been reported thus far. Accordingly, we validated our *swell-and-click* approach by testing the SPAAC reaction between the alkylated VLPs, PhMV-yne (1 mg/mL, 0.1 wt%), and the azide monomer (AC-PEG2K–N_3) at increasing concentrations (0, 10, 50, 100 mg/mL, the latter being the monomer concentration present during hydrogel synthesis). As a control, the same reaction was prepared using PhMV-cy5.5 (lacking the alkyne handle). As expected, electrophoresis showed no evidence of a *click* reaction between PhMV-cy5.5 and the azide monomer, regardless of the monomer concentration. Only PhMV CPs (~20 kDa) were detected by denaturing SDS-PAGE (Fig. S1A left). Conversely, two CP bands were observed by denaturing SDS-PAGE when PhMV-yne was mixed with the azide monomer (Fig. S1A, right). These represented the normal PhMV CP and a higher-molecular-weight version carrying the AC-PEG-N_3 linker (MW 2 kDa). Comparative analysis of these bands using ImageJ software indicated that 230–270 lysines per VLP undergo SPAAC with the azide monomer, approximately one third of available lysines. The *click* reaction was also confirmed by native electrophoresis, where the *clicked* particles showed lower mobility than PhMV-yne due to the higher radius after functionalization (Fig. S1B, right). Interestingly, this preliminary test showed that *click* chemistry between PhMV-yne and AC-PEG2K–N_3 was successful even at 10-fold lower azide concentrations (10 mg/mL) than those used for the hydrogel synthesis (100 mg/mL). Changes in migration were not observed for PhMV-cy5.5 in native electrophoresis experiments because no reaction takes place between these particles and the AC-PEG2K–N_3 monomer (Fig. S1B, left).

3.3. Characterization of control hydrogels and VLP-laden hydrogels

3.3.1. VLP loading test

The simplest way to validate the *swell-and click* method is a VLP loading test, which determines the maximum efficiency of the hydrogels to incorporate VLPs during swelling. Previous reports show that hydrogels can react during swelling when the reactants are present in the same aqueous solution [32]. Success in the loading test is mainly determined by the chemical reactivity of the hydrogel and VLP, as well as VLP solubility and concentration in the swelling solution [33].

We immersed a fully dried HG xerogel in a large volume of VLP solution to cover several times the maximum swelling capacity (SD_{max}) of the HG (e.g., 5 mL for a xerogel with a mass of 70–100 mg). The PhMV-cy5.5 and PhMV-yne solutions were tested at initial concentrations of C_i = 0.1, 0.5 and 0.75 mg/mL (0.01, 0.05 and 0.075 wt%, respectively). We then calculated SD_{max} for the hydrogel in the VLP solution and the VLP loading after the swelling process. The SD_{max} is the percentage weight gain in water and VLP of a hydrogel after full swelling and is calculated using the equation $SD = [(W_S–W_0)/W_0] \times 100$, where W_S and W_0 are the weights of the fully swollen and fully dried hydrogels, respectively. VLP loading is calculated by UV/vis analysis (λ_{Cy5} = 675 nm) of the VLP swelling solution using the formula *VLP loading (%)* = $[(M_t\text{-}M_u)/M_t]$*100, where M_t and M_u are the total mass of VLPs added and the total unloaded VLP mass remaining in the supernatant, respectively. UV/VIS spectroscopic data can be found in Fig. S2.

Fig. 3A shows the SD_{max} of the HG in each VLP solution. The SD_{max} was roughly the same for both VLPs, which means the hydrogel always incorporates the same mass of water regardless of the VLP type. However, the SD_{max} declined slightly as the VLP concentration increased (SD_{max} = 2480 ± 28 %, 2124 ± 8.0 % and 1954 ± 1.5 wt% for PhMV-cy5.5 at C_i = 0.1, 0.5 and 0.75 mg/mL, respectively; SD_{max} = 2408 ± 75 %, 2136 ± 24 % and 1979 ± 87 wt% for PhMV-yne at C_i = 0.1, 0.5 and 0.75 mg/mL, respectively). This typical trend is observed in hydrogel swelling studies whereby increasing the concentration of the swelling solution leads to lower swelling ratios [34].

Conversely, the loading percentage clearly differed between the two VLPs (Fig. 3B). The *clickable* alkyne-modified VLP achieved higher loading values of 46.2 %, 56.2 % and 34.7 % at C_i = 0.1, 0.5 and 0.75 mg/mL, respectively, compared to the PhMV-cy5.5 control with values of 33.3 %, 42.2 % and 15.5 % at the same initial concentrations. At C_i = 0.75 mg/mL, the loading value of PhMV-yne was more than double that of PhMV-cy5.5, whereas the difference was only 1.3–1.4-fold at lower VLP concentrations. This suggests VLP loading is a function of both the VLP chemistry and C_i. The higher VLP loading observed for PhMV-yne indicates that the particles undergo a *click* reaction with the hydrogel during swelling, even at VLP concentrations as low as 0.1 mg/mL (0.01 wt%), confirming the suitability of the *swell-and-click* approach.

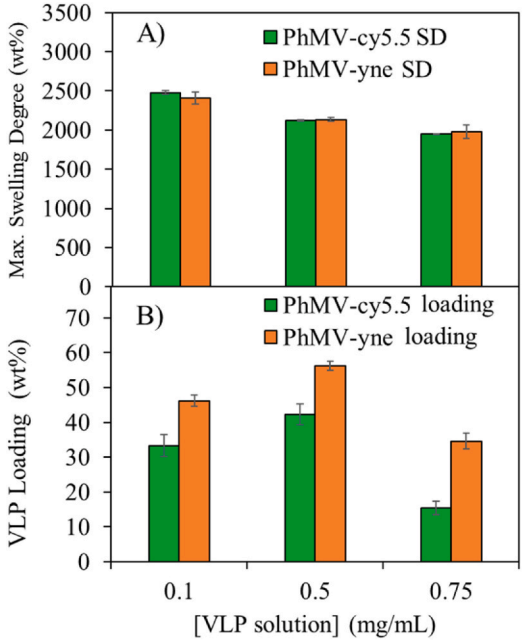

Fig. 3. VLP loading test for the control hydrogel (HG): A) SD_{max} and B) VLP loading.

3.3.3. Mechanical properties

As previously stated, the PhMV-yne VLP is highly multivalent, with 230–270 *clicked* junctions per particle and thus has a high potential to crosslink the polymeric network. We therefore compared the mechanical and rheological properties of the HG and VHGs in compressive strength and frequency sweep tests. These provide insight into the stiffness and viscoelasticity of the materials, both of which are influenced by the degree of crosslinking [39,40].

Compressive strength studies involved the application of a uniaxial load to cylindrical hydrogel samples -prepared by swelling the corresponding xerogels in 100 μL PBS- causing them to shorten and spread laterally (Fig. 5A). Hydrogel disk samples were compressed in this manner until ε = 75 % strain (*i.e.,* 75 % sample height) for five consecutive cycles. After compression, the HG and VHG samples fully regained their original shape without breaking, thus proving the mechanical integrity of both HG and VHGs. The average compressive cycles were then plotted as a stress–strain curve (Fig. 5B).

The compressive stress at maximum strain (ε = 70 %) of the VHGs was somewhat lower than that of the control HG, reaching values of 66, 59 and 54 kPa for the HG, VN-HG and VC-HG, respectively (Fig. 5B). In the ε = 0–10 % region, the Young's modulus (*E*) can be extracted from the slope of the stress–strain curve (Fig. 5B inset). This was similar for the HG (16.3 ± 5.68 kPa) and VN-HG (15.97 ± 4.89 kPa), but lower for the VC-HG (12.57 ± 6.02 kPa). These results show that the incorporation of VLPs into the HG produces more elastic, low-moduli materials. Typically, hydrogels with lower moduli and higher elasticities translate into less compact, loosely crosslinked networks [41]. In our VHG systems, despite the multivalent crosslinking sites of the alkynylated VLP, the latter does not appear to crosslink the hydrogel network at this VLP concentrations (1 mg/mL, 0.1 wt%). Rather, we hypothesize the particle covalently functionalizes the HG network without network stiffening.

Rheological analysis under the same compressive conditions was followed by a frequency sweep in the range ω = 0–100 rad/s. We plotted the storage modulus (G′) and loss modulus (G″) against the oscillation frequency (Fig. S5A). Throughout the frequency range, G′ > G″ with no crossover point for all three hydrogels, the typical correlation observed for solid-like, fully crosslinked hydrogels [42]. The phase angle or loss tangent (δ) increased from 5° to 25° for all samples throughout the frequency range, which indicates that all hydrogels transition slightly from elastic to somewhat viscoelastic materials (Fig. S5B). The HG and VHGs both behave as similarly crosslinked, solid-like materials that retain their integrity even following high stress.

The rheological and mechanical tests indicated that the incorporation of the VLPs has a low mechanical impact on the HG, probably reflecting the post-synthesis *swell-and-click* method. Because the VLPs are swollen and *clicked* into the HG only after the latter has been crosslinked by PEGDA and the degree of crosslinking has been fixed during synthesis, the VLPs do not appear to contribute significantly to further crosslinking at this VLP concentrations (1 mg/mL, 0.1 wt%), despite their multivalency. This contrasts with previous *in situ* VLP crosslinking methods, where the covalent binding of VLPs in the hydrogel increased the mechanical strength of the materials [14,15,19], ultimately limiting the number of VLPs that can be loaded and thus potentially interfering with the ability to match the required therapeutic window in clinical settings.

3.3.2. Thermogravimetric analysis

Thermogravimetric analysis (TGA) measures the change in mass of a sample over time as the temperature changes. Given that the thermal stability of a material strongly depends on its chemical structure, we can infer the presence of new chemical bonds by thermal decomposition. Furthermore, differential thermograms (DTGs) reveal subtle differences between TGA profiles. We therefore prepared DTGs for the monomers, HG and VLPs to identify the chemical nature of each temperature loss (Fig. 4) and then analyzed the DTGs of the VHGs (Fig. 5). The full range thermograms (TGs) and DTGs of the former and latter groups can be found in Fig. S3 and Fig. S4, respectively. Further, each weight loss and temperature are summarized in chart S1.

The DTGs of the HG and its monomeric components AAm and AC-PEG2K–N_3 were plotted in the range 250–450 °C (Fig. 4A) along with the corresponding thermograms (Fig. S3). The HG showed a shoulder-like loss at 295 °C that matches the AAm monomer and this reflects intramolecular decomposition reactions in the polyacrylamide backbone [35]. A second loss at 390 °C was attributed to the AC-PEG2K–N_3 monomer as well as the C–C main backbone in AAm [36,37]. The presence of both monomers in the HG backbone confirmed the structure of the hydrogel (Fig. 4A).

The DTGs of the VLPs were plotted in the range 150–450 °C (Fig. 4B).

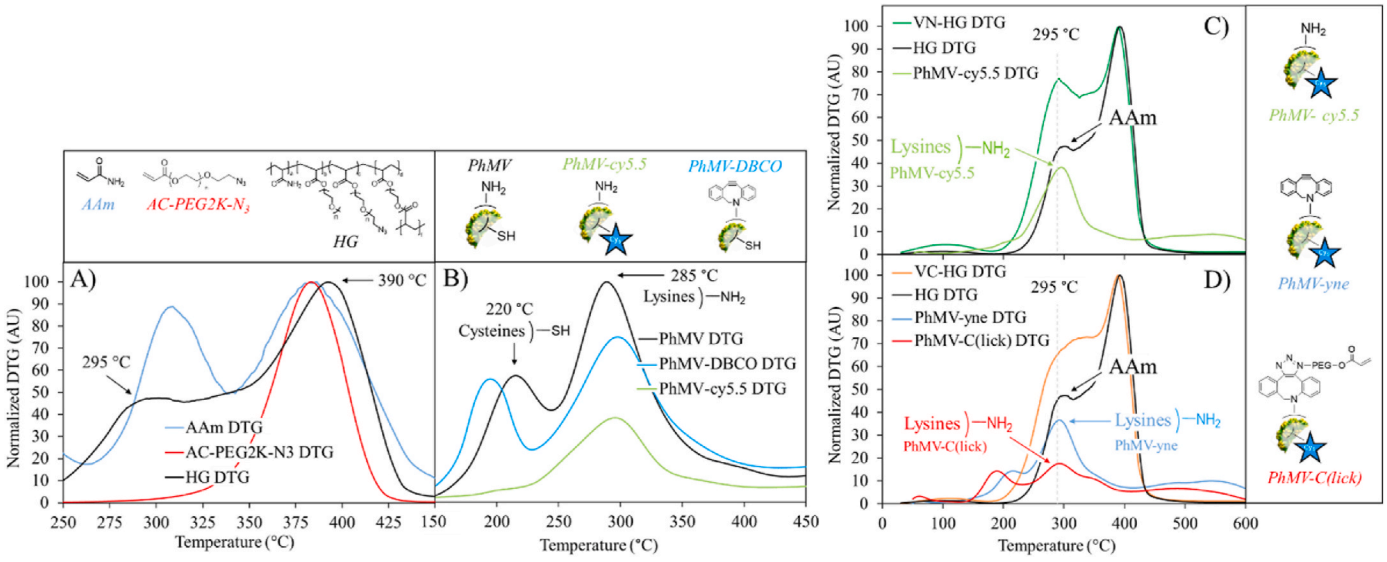

Fig. 4. Differential thermograms (DTGs) for the control hydrogel (HG), the VLP-laden hydrogels (VHGs) and their respective components. A) Acrylamide (AAm, blue), AC-PEG2K–N_3 (red) and HG (black) in the range 250–450 °C. B) PhMV (black), PhMV-DBCO (blue) and PhMV-cy5.5 (green) VLPs in the range 150–450 °C. C) The VLP-native hydrogel (VN-HG, dark green), HG (black) and PhMV-cy5.5 (light green) in the range 0–600 °C. D) The VLP-*clicked* hydrogel (VC-HG, orange), HG (black), PhMV-yne (blue) and PhMV-C(lick) (red) in the range 0–600 °C. Chemical structures of the monomers, HG and simplified VLP structures are shown next to the figures. (For interpretation of the references to color in this figure legend, the reader is referred to the Web version of this article.)

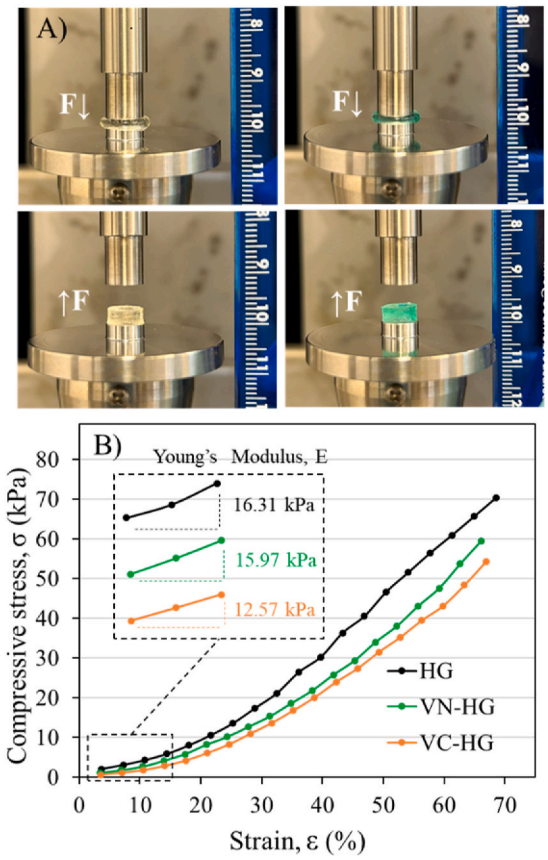

Fig. 5. Compressive strength of the control hydrogel (HG) and VLP-laden hydrogel (VHG) samples. A) Experimental setup. B) Compressive stress–strain curves and Young's modulus (inset).

The DTG of PhMV showed losses at 220 and 285 °C. The loss at 220 °C was barely apparent for PhMV-cy5.5, indicating it is caused by thermal decomposition of the free cysteine residues in PhMV. These residues are covalently conjugated to the maleimide dye in PhMV-cy5.5, which improves their thermal stability and reduces the magnitude of the loss. The second loss at 285 °C was partially quenched in PhMV-DBCO, indicating this loss is caused by the thermal decomposition of free lysine residues. Their thermal stability increases when they are conjugated to NHS esters, also reducing the peak loss. As expected, the cysteine loss at 220 °C in PhMV-DBCO is unchanged because no cysteines were conjugated in this VLP.

Further evidence of VLP conjugation can be observed in the high-temperature region (Fig. S3). The loss at 880 °C in PhMV, probably caused by decomposition of the protein backbone [38], notably increases in PhMV-DBCO and PhMV-cy5.5. This accelerated thermal decomposition in the conjugated VLPs is consistent with a higher number of ester and thiosuccinimide bonds (the end products of lysine and cysteine conjugation, respectively) in the polypeptide backbone, which decompose in the high-temperature range.

The DTGs of the VN-HG, HG and PhMV-cy5.5 (Fig. 4C) show that the VN-HG (the result of incorporating PhMV-cy5.5 into the HG) shares a very similar thermal profile with the precursor HG, with two main losses at 295 and 390 °C. The 390 °C loss in VN-HG can be attributed solely to the HG polymer backbone, although the 295 °C loss can be deconvoluted into the AAm loss corresponding to the amide groups in the HG and the loss attributed to the lysine residues in the PhMV-cy5.5 particle at 285 °C. Due to the co-decomposition of both groups at this temperature, the loss at 295 °C is greater in VN-HG than in HG and PhMV-cy5.5 alone.

Fig. 4D shows the DTGs of the VC-HG (the result of incorporating PhMV-yne into the HG), HG, PhMV-yne (including the free alkyne bond) and PhMV-C(lick), wherein the alkyne bond has undergone SPAAC with an azide monomer. Interestingly, the loss at 295 °C is partially quenched in the VC-HG compared to the VN-HG, which indicates the VC-HG is thermally more stable than the VN-HG at this temperature. Given the same AAm contribution in both hydrogels, this improvement in thermal stability can only be attributed to difference in the VLP. In the VC-HG, the alkynylated VLP can exist either as a non-*clicked* VLP or *clicked* to the azide pendant groups. By comparing the thermal profiles of these VLPs, it is clear the lysine loss in PhMV-C(lick) is lower than in PhMV-yne, which indicates the *clicked* PhMV is thermally more stable than its non-*clicked* counterpart. The reduced loss at 295 °C for the VC-HG compared to the VN-HG therefore indicates that PhMV exists in the *clicked* state inside the hydrogel, which increases the thermal stability of the lysines and reduces the overall signal loss of VC-HG at this temperature. These findings agree with the previous VLP loading studies and support the use of our *swell-and-click* approach.

3.3.4. Swelling and porosity studies

The swelling degree (SD) of a hydrogel is defined as its capacity to incorporate water within its porous structure [43]. SD and microporosity are two interconnected parameters, along with the mechanical properties, which can indicate whether VLPs exert any crosslinking effect. Typically, hydrogels with a high degree of crosslinking result in more compact networks with smaller pores, reducing the SD [44]. We investigated the SD of the hydrogels over time using a gravimetric method. First, we immersed the fully dried HG, VC-HG and VN-HG xerogels in water and measured their weights at different time points, according to the formula $SD = [(W_T\text{-}W_0)/W_0] \times 100$, where W_T and W_0 are the weights of the swollen hydrogel at time T and time T = 0, respectively. The SD values are plotted in Fig. 6.

Burst swelling was observed for all hydrogels during the first day, but a plateau was reached on the third day, with slightly higher SD values for the HG (1800 ± 16 wt%), followed by the VN-HG (1760 ± 15 wt%) and VC-HG (1700 ± 58 wt%). The lower SD value for the VC-HG suggests the alkynylated particle exerts some crosslinking effect in the hydrogel, albeit to a negligible extent given the small difference compared to the VN-HG. A similar conclusion can be drawn from the maximum swelling (SD_{max}), where HG xerogels became swollen in the PhMMV-cy5.5 and PhMV-yne solutions at increasing concentrations (Fig. 3A). There was no decrease in SD_{max} values over the entire VLP concentration range (0.1–0.75 mg/mL) when the HG was swollen in the PhMV-yne solution compared to PhMV-cy5.5, indicating that the alkynylated VLP, despite its multivalency, does not increase the degree of hydrogel crosslinking.

These phenomena can be explained by the *swell-and-click* approach we used to incorporate the VLPs, which takes place once the crosslinking degree of the hydrogel has been fixed during synthesis, and therefore

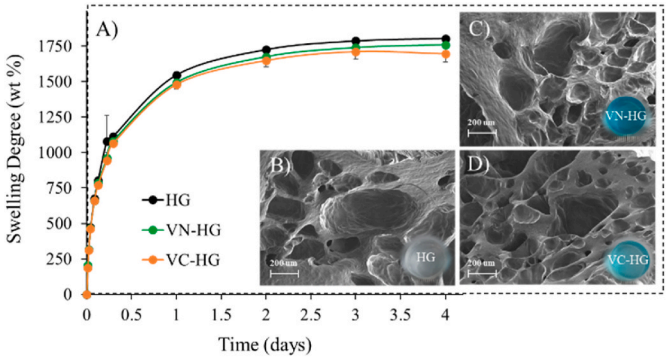

Fig. 6. Swelling and porosity studies. A) Swelling degree (SD) of the control hydrogel (HG) and VLP-laden hydrogels (VN-HG, VC-HG) samples in water. Pore sizes for B) HG, C) VN-HG (incorporating native PhMV particles) and D) VC-HG (incorporating VLP-clicked particles).

determines beforehand both the mechanical and swelling properties of the materials.

The porosity of the maximally swollen hydrogels was determined by scanning electron microscopy (SEM). All three hydrogels formed a microporous network with pore sizes in the same range: 251.3 ± 137.8 μm for HG, 200.8 ± 109.9 μm for VN-HG and 226.2 ± 116.2 μm for VC-HG. The morphology of the pores was heterogeneous, as typically observed for free-radical polymerized hydrogels [45]. In agreement with the SD data and mechanical properties, the similar pore dimensions and morphologies imply similar degrees of crosslinking independent of VLP functionalization. These results confirm that the *swell-and-click* post-synthesis approach has advantages over *in situ* VLP crosslinking methods where the VLPs are incorporated during polymer synthesis because our method did not affect significantly hydrogel properties such as swellability, porosity or mechanical consistency at the current studied VLP range (0.1–1 mg/mL, 0.01–0.1 wt%). It is thus possible that a greater quantity of VLP cargo was covalently attached to the hydrogel without over-stiffening the network or compromising the hydrophilicity and pore sizes.

3.3.5. FTIR spectroscopy

FTIR spectroscopy of all three samples HG, VN-HG and VC-HG revealed that the most intense bands can be attributed to C–C (2874 cm^{-1}) and C–O stretch (1088 cm^{-1}) from the PEG moiety [46], which is abundant in both the PEGMA and AC-PEG-N_3 monomers (Fig. S6A). Carbonyl C═O strong bands were also detected for acrylate esters (1727 cm^{-1}) and acrylamide (1660 cm^{-1}), as well as the N–H stretching for the latter (3450–3170 cm^{-1}) [47]. Intense free azide N═N═N bands (here, 2101 cm^{-1}) are reported to disappear following successful click chemistry [48]. However, in our system, the N_3 stretch was too weak to reveal any proof of such reaction. This reflects the PEG-rich composition of the AC-PEG-N_3 commercial monomer used in our hydrogels, which dwarfed the C═O and N═N═N bands, as seen in the spectra for the AC-PEG-N_3 monomer (MW 2 kDa) and even at lower PEG weights (MW 1 kDa) (Fig. S6B).

3.4. In vitro VLP release experiments

VLPs are used to develop vaccines targeting chronic diseases and cancer due to their potent immunogenicity [49]. However, long-term treatment is a challenge where repeated administration is required [50]. We therefore tested our VHGs as proof-of-concept long-term reservoirs to release VLPs in a sustained manner. In our VHG systems, the robust triazole bond binding the VLP to the hydrogel is not broken or hydrolyzed [51], but the ester bonds in the PEG backbone gradually break under mildly alkaline conditions [52]. PEGylated VLPs would therefore be released from the hydrogel as the latter slowly degrades over time, allowing the sustained release of the VLPs over a period of months.

HG xerogels (70–100 mg, SD_{max}=0 wt%) were swollen in 5 mL of the PhMV-yne or PhMV-cy5.5 solutions at a fixed concentration (C_i = 0.75 mg/mL, 0.075 wt%) until they reached the maximum swollen state (W_0 = 1950–1990 mg, SD_{max}=1950–1980 wt%) (Fig. S7), following the same protocol used for VLP loading (Fig. 3). A baseline control HG xerogel was swollen in PBS. All maximum-swollen hydrogels were then immersed in fresh PBS under stirring and protected from light. At specific time points, an aliquot was withdrawn for UV/vis spectrophotometry ($\lambda_{cy5.5}$ = 675 nm) and the aliquot was returned to the supernatant to keep the final volume constant.

The cumulative release of VLPs from the hydrogels is plotted in Fig. 7. Nearly 100 % of the PhMV-cy5.5 VLPs were released from the VN-HG in a burst process after the first 24 h, whereas only 49.6 % of the PhMV-yne VLPs were released from the VC-HG, plateauing afterwards (Fig. 7A). This sharp difference further suggests covalent attachment between the alkynylated VLPs and the hydrogel, and thus corroborates the success of the *swell-and-click* approach. However, about half of the alkyne VLP cargo was burst-released during the first day, and these are probably alkynylated VLPs that did not *click* successfully during the VLP loading step, but instead simply diffused into the HG. Given that PhMV-yne loading at C_i = 0.75 mg/mL was 34.7 %, and the released VLPs represented 49.6 % of that load, the actual load of *clicked* PhMV-yne VLPs in the hydrogel can be calculated after release as C_{VLPs} = [34.7 % × (100–49.6 %)]/100 = 17.5 %. It follows that 17.5 % of all the PhMV-yne particles added during the loading step remained *clicked* to the hydrogel even after 2 weeks. After that time and having reached a steady release profile, all released PhMV-yne VLPs are presumed to be in equilibrium with the release medium, and thus the hydrogels were immersed again in fresh buffer to encourage the release of the remaining loaded VLPs and study the month-term release (Fig. 7B). After this additional buffer immersion (t = ½ months), a milder ~10 % burst VLP release was observed for VC-HG, which gradually increased until reaching 63 % release of PhMV-yne VLPs after 2 months. These findings also highlight the suitability of the *swell-and-click* approach to successfully fabricate, for the first time, long-term VLP release reservoirs.

The successful *click* of the VLPs significantly reduced the burst release during the early hours of the experiment (Fig. S8), with >30 % of the PhMV-cy5.5 VLPs released from the VN-HG after the first hour and 65 % after the seventh hour, in contrast to only ~16 % and ~37 % of the PhMV-yne VLPs released from the VC-HG at the same time points. While burst release often leads to premature cargo loss and unwanted side effects [53], in immunotherapy/vaccine development the initial burst release is viewed as a positive trait – it mimics the "prime" while the

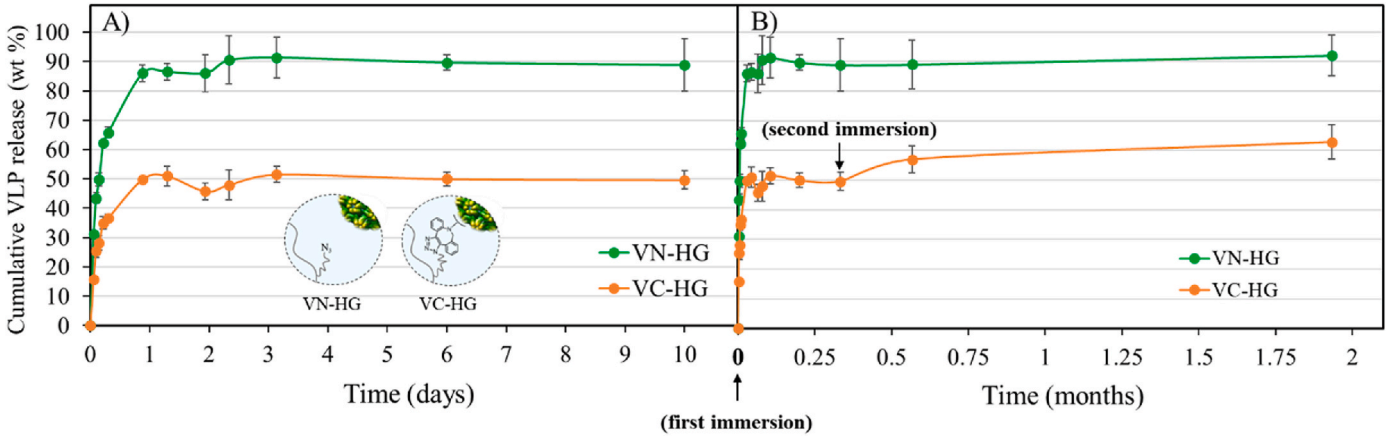

Fig. 7. Cumulative release of VLPs from VLP-laden hydrogels in vitro. A) weekly release B) monthly release.

sustained release then mimics the multiple "boosts" but built into a single formulation and administration. The present VC-HG hydrogel therefore achieves both, burst release to kick-start the immune system followed by slow-release for sustained efficacy in the time-scale of weeks to months, which is favorable for the desired application.

Finally, we investigated the structural integrity of the VLPs after release from the hydrogels. We used UV/vis spectrophotometry, which has a low detection limit suitable for highly diluted particles. In the 195–295 nm range, the spectra of the released PhMV-cy5.5 and PhMV-yne VLPs were similar to their counterparts prior to loading and distinct from the profiles of denatured VLPs (Figs. S9A and B). This confirmed that the released VLPs from the hydrogels were not denatured and retained full structural integrity. In the 530–730 nm range, the UV/vis spectra of the conjugated cy5.5 dye in the VLPs ($\lambda_{cy5.5} = 675$ nm) was also preserved after release (Figs. S9C and D), which confirmed that conjugated cy5.5 is not chemically modified after leaving the hydrogel and the UV/vis absorbance readings are therefore reliable. The *swell-and-click* approach thus allows the covalent bonding of VLPs to a hydrogel without altering the consistency and properties of the scaffold and facilitating the slow release of the cargo. Previously reported *in situ* VLP crosslinking methods required a minimum viral concentration of 5–10 mg/mL (0.5–1 wt%) for the hydrogel to gelate consistently [14,15,19]. In the *swell-and-click* approach, hydrogel gelation is independent of VLP functionalization, and the minimum VLP load that can be covalently attached to the hydrogel is dependent only on the detection limit of the instrumentation used to quantify particle loading and release, which in this study was as low as 0.1 mg/mL (0.01 wt%).

4. Conclusions

For the first time, we have achieved the covalent binding of VLPs to a hydrogel by exploiting its swellability using a novel *swell-and-click* approach, and thus circumvent the need for high viral loadings to achieve hydrogel gelation. Azide-functionalized, mechanically stable hydrogels readily swell in an aqueous VLP solution, during which alkyne VLPs bind to the hydrogel scaffold *via* copper-free *click* chemistry. We confirmed covalent functionalization of the VLPs with loadings as low as 0.1–1 mg/mL (0.01–0.1 wt%) and no apparent changes in the hydrophilicity, mechanical stability, viscoelasticity or microporosity of the hydrogels despite the potential for VLPs to form additional crosslinks. This implies the VLPs do not likely contribute to further crosslinking, which instead is mainly attributed to PEGDA. Further, the *swell-and-click* protocol more than doubled the VLP loadings in the hydrogel, and sequentially combined an initial burst VLP release followed by a month-sustained release, both of which are desired for cancer immunotherapy treatment. Our novel methodology outperforms the previous synthetic approaches in that VLP loadings and hydrogel mechanical stability can now be controlled independently, leading to mechanically stable, long-term release VLP reservoirs. This promising *swell-and-click* approach facilitates the scalability of the fabrication process and moves a significant step forward towards clinical translation of long-term VLP vaccination in cancer disease.

Associated content

Validity electrophoresis test of SPAAC reaction for PhMV-cy5.5 and PhMV-yne (Fig. S1). UV/VIS spectroscopic data for VLP loading and release experiments (Fig. S2). Thermograms and differential thermograms in the 0–1200 °C range (Figs. S3 and S4). Summary of weight and temperature for each TG loss (Chart S1). Rheology test under frequency sweep conditions (Fig. S5). FTIR spectra of the control hydrogel and VLP-laden hydrogel samples and AC-PEG1K–N3 and AC-PEG2K–N3 monomer (Fig. S6). Digital pictures of control hydrogel and VLP-laden hydrogels before in vitro release (Fig. S7). Burst VLP release from VLP hydrogels during early hours. (Fig. S8). UV/vis spectra of VLPs before and after release from the hydrogel (Fig. S9).

CRediT authorship contribution statement

Jorge Leganés Bayon: Writing – review & editing, Writing – original draft, Visualization, Validation, Methodology, Investigation, Conceptualization. **Calvin Shih:** Validation, Investigation. **Stephen L. Craig:** Funding acquisition, Writing – review & editing. **Nicole F. Steinmetz:** Writing – review & editing, Supervision, Resources, Funding acquisition, Conceptualization, Project administration.

Declaration of competing interest

The authors declare the following financial interests/personal relationships which may be considered as potential competing interests: Jorge Leganes reports financial support and travel were provided by National Science Foundation. Jorge Leganes has patent pending to Assigne UC San Diego. If there are other authors, they declare that they have no known competing financial interests or personal relationships that could have appeared to influence the work reported in this paper.

Data availability

Data will be made available on request.

Acknowledgements

This work was supported by the NSF Center for the Chemistry of Molecularly Optimized Networks (MONET), CHE-2116298. The authors acknowledge the use of facilities and instrumentation supported by NSF through the UC San Diego Materials Research Science and Engineering Center (UCSD MRSEC), grant DMR-2011924. This work was performed in part at the San Diego Nanotechnology Infrastructure (SDNI) of the University of California, San Diego, a member of the National Nanotechnology Coordinated Infrastructure (NNCI), which is supported by the National Science Foundation (grant ECCS-1542148). The authors thank the University of California, San Diego Cellular and Molecular Medicine Electron Microscopy Core (UCSD-CMM-EM Core, RRID: SCR_022039) for equipment access and technical assistance. The UCSD-CMM-EM Core is partly supported by the National Institutes of Health award number S10OD023527.

Appendix A. Supplementary data

Supplementary data to this article can be found online at https://doi.org/10.1016/j.mtchem.2024.102100.

References

[1] K.J. Koudelka, A.S. Pitek, M. Manchester, N.F. Steinmetz, Virus-based nanoparticles as Versatile nanomachines, Annu Rev Virol 2 (2015) 379–401, https://doi.org/10.1146/annurev-virology-100114-055141.
[2] Y.H. Chung, H. Cai, N.F. Steinmetz, Viral nanoparticles for drug delivery, imaging, immunotherapy, and theranostic applications, Adv. Drug Deliv. Rev. 156 (2020) 214–235, https://doi.org/10.1016/j.addr.2020.06.024.
[3] G. Valdivia, D. Alonso-Miguel, M.D. Perez-Alenza, A.B.E. Zimmermann, E. Schaafsma, F.W. Kolling, L. Barreno, A. Alonso-Diez, V. Beiss, J.F. Affonso de Oliveira, M. Suárez-Redondo, S. Fiering, N.F. Steinmetz, J. vom Berg, L. Peña, H. Arias-Pulido, Neoadjuvant intratumoral immunotherapy with cowpea mosaic virus induces local and systemic antitumor efficacy in canine mammary cancer patients, Cells 12 (2023) 2241, https://doi.org/10.3390/cells12182241.
[4] M.O. Mohsen, M.F. Bachmann, Virus-like particle vaccinology, from bench to bedside, Cell. Mol. Immunol. 19 (2022) 993–1011, https://doi.org/10.1038/s41423-022-00897-8.
[5] A.A. Wright, A. Cronin, D.E. Milne, M.A. Bookman, R.A. Burger, D.E. Cohn, M. C. Cristea, J.J. Griggs, N.L. Keating, C.F. Levenback, G. Mantia-Smaldone, U. A. Matulonis, L.A. Meyer, J.C. Niland, J.C. Weeks, D.M. O'Malley, Use and effectiveness of intraperitoneal chemotherapy for treatment of ovarian cancer, J. Clin. Oncol. 33 (2015) 2841–2847, https://doi.org/10.1200/JCO.2015.61.4776.
[6] J. Li, D.J. Mooney, Designing hydrogels for controlled drug delivery, Nat. Rev. Mater. 1 (2016) 16071, https://doi.org/10.1038/natrevmats.2016.71.
[7] P. Jiménez-Rosado, M. Romero, Novel trends in hydrogel development for biomedical applications: a review, Polymers 2022 (2022) 3023, https://doi.org/10.3390/polym.

[8] A. Singh, N.A. Peppas, Hydrogels and scaffolds for immunomodulation, Adv Mater 26 (2014) 6530–6541, https://doi.org/10.1002/adma.201402105.

[9] S. Emoto, H. Yamaguchi, T. Kamei, H. Ishigami, T. Suhara, Y. Suzuki, T. Ito, J. Kitayama, T. Watanabe, Intraperitoneal administration of cisplatin via an in situ cross-linkable hyaluronic acid-based hydrogel for peritoneal dissemination of gastric cancer, Surg. Today 44 (2014) 919–926, https://doi.org/10.1007/s00595-013-0674-6.

[10] Y. Umeki, K. Mohri, Y. Kawasaki, H. Watanabe, R. Takahashi, Y. Takahashi, Y. Takakura, M. Nishikawa, Induction of potent antitumor immunity by sustained release of cationic antigen from a DNA-based hydrogel with adjuvant activity, Adv. Funct. Mater. 25 (2015) 5758–5767, https://doi.org/10.1002/adfm.201502139.

[11] G.W. Ashley, J. Henise, R. Reid, D.V. Santi, Hydrogel drug delivery system with predictable and tunable drug release and degradation rates, Proc Natl Acad Sci U S A 110 (2013) 2318–2323, https://doi.org/10.1073/pnas.1215498110.

[12] E.C. Gale, A.E. Powell, G.A. Roth, E.L. Meany, J. Yan, B.S. Ou, A.K. Grosskopf, J. Adamska, V.C.T.M. Picece, A.I. d'Aquino, B. Pulendran, P.S. Kim, E.A. Appel, Hydrogel-based slow release of a receptor-binding domain subunit vaccine elicits neutralizing antibody responses against SARS-CoV-2, Adv. Mater. 33 (2021), https://doi.org/10.1002/adma.202104362.

[13] C. Dickmeis, L. Kauth, U. Commandeur, From infection to healing: the use of plant viruses in bioactive hydrogels, Wiley Interdiscip Rev Nanomed Nanobiotechnol 13 (2021), https://doi.org/10.1002/wnan.1662.

[14] L. Yang, A. Liu, M.V. De Ruiter, C.A. Hommersom, N. Katsonis, P. Jonkheijm, J.J.L. M. Cornelissen, Compartmentalized supramolecular hydrogels based on viral nanocages towards sophisticated cargo administration, Nanoscale 10 (2018) 4123–4129, https://doi.org/10.1039/c7nr07718a.

[15] L. Chen, X. Zhao, Y. Lin, Z. Su, Q. Wang, Dual stimuli-responsive supramolecular hydrogel of bionanoparticles and hyaluronan, Polym. Chem. 5 (2014) 6754–6760, https://doi.org/10.1039/c4py00819g.

[16] C.I. Nkanga, O.A. Ortega-Rivera, M.D. Shin, M.A. Moreno-Gonzalez, N. F. Steinmetz, Injectable slow-release hydrogel formulation of a plant virus-based COVID-19 vaccine candidate, Biomacromolecules 23 (2022) 1812–1825, https://doi.org/10.1021/acs.biomac.2c00112.

[17] M.A. Bruckman, G. Kaur, A.L. Lee, F. Xie, J. Sepulveda, R. Breitenkamp, X. Zhang, M. Joralemon, T.P. Russell, T. Emrick, Q. Wang, Surface modification of tobacco mosaic virus with "click" chemistry, Chembiochem 9 (2008) 519–523, https://doi.org/10.1002/cbic.200700559.

[18] X. Qiu, X. Kang, J. Zhu, L. Yi, Chemical labeling and crosslinking of tobacco mosaic virus via multi-diazonium reagents: examples, applications, and prospects, Mater Adv 3 (2022) 5248–5259, https://doi.org/10.1039/d2ma00311b.

[19] D. Ma, J. Zhang, C. Zhang, Y. Men, H. Sun, L.Y. Li, L. Yi, Z. Xi, A highly efficient dual-diazonium reagent for protein crosslinking and construction of a virus-based gel, Org. Biomol. Chem. 16 (2018) 3353–3357, https://doi.org/10.1039/c8ob00169c.

[20] D.C. Schoenmakers, L. Schoonen, M.G.T.A. Rutten, R.J.M. Nolte, A.E. Rowan, J.C. M. Van Hest, P.H.J. Kouwer, Virus-like particles as crosslinkers in fibrous biomimetic hydrogels: approaches towards capsid rupture and gel repair, Soft Matter 14 (2018) 1442–1448, https://doi.org/10.1039/c7sm02320k.

[21] A. Southan, T. Lang, M. Schweikert, G.E.M. Tovar, C. Wege, S. Eiben, Covalent incorporation of tobacco mosaic virus increases the stiffness of poly(ethylene glycol) diacrylate hydrogels†, RSC Adv. 8 (2018) 4686–4694, https://doi.org/10.1039/c7ra10364f.

[22] R.M. Abaskharon, F. Gai, Direct measurement of the tryptophan-mediated photocleavage kinetics of a protein disulfide bond, Phys. Chem. Chem. Phys. 18 (2016) 9602–9607, https://doi.org/10.1039/c6cp00865h.

[23] C. Dickmeis, L. Kauth, U. Commandeur, From infection to healing: the use of plant viruses in bioactive hydrogels, Wiley Interdiscip Rev Nanomed Nanobiotechnol 13 (2021), https://doi.org/10.1002/wnan.1662.

[24] K.J. Barkovich, Z. Zhao, N.F. Steinmetz, iRGD-targeted physalis mottle virus like nanoparticles for targeted cancer delivery, Small Science 3 (2023), https://doi.org/10.1002/smsc.202300067.

[25] K.J. Barkovich, Z. Wu, Z. Zhao, A. Simms, E.Y. Chang, N.F. Steinmetz, Physalis mottle virus-like nanocarriers with expanded internal loading capacity, Bioconjug Chem (2023), https://doi.org/10.1021/acs.bioconjchem.3c00269.

[26] S.I. Presolski, V.P. Hong, M.G. Finn, Copper-catalyzed azide–alkyne click chemistry for bioconjugation, Curr Protoc Chem Biol 3 (2011) 153–162, https://doi.org/10.1002/9780470559277.ch110148.

[27] K.G. Patel, J.R. Swartz, Surface functionalization of virus-like particles by direct conjugation using azide-alkyne click chemistry, Bioconjug Chem 22 (2011) 376–387, https://doi.org/10.1021/bc100367u.

[28] E. Kim, H. Koo, Biomedical applications of copper-free click chemistry:: in vitro, in vivo, and ex vivo, Chem. Sci. 10 (2019) 7835–7851, https://doi.org/10.1039/c9sc03368h.

[29] H. Masarapu, B.K. Patel, P.L. Chariou, H. Hu, N.M. Gulati, B.L. Carpenter, R. A. Ghiladi, S. Shukla, N.F. Steinmetz, Physalis mottle virus-like particles as nanocarriers for imaging reagents and drugs, Biomacromolecules 18 (2017) 4141–4153, https://doi.org/10.1021/acs.biomac.7b01196.

[30] H. Masarapu, B.K. Patel, P.L. Chariou, H. Hu, N.M. Gulati, B.L. Carpenter, R. A. Ghiladi, S. Shukla, N.F. Steinmetz, Physalis mottle virus-like particles as nanocarriers for imaging reagents and drugs, Biomacromolecules 18 (2017) 4141–4153, https://doi.org/10.1021/acs.biomac.7b01196.

[31] H. Hu, H. Masarapu, Y. Gu, Y. Zhang, X. Yu, N.F. Steinmetz, Physalis mottle virus-like nanoparticles for targeted cancer imaging, ACS Appl. Mater. Interfaces 11 (2019) 18213–18223, https://doi.org/10.1021/acsami.9b03956.

[32] J. Leganés, A.M. Rodríguez, M.A. Arranz, C.A. Castillo-Sarmiento, I. Ballesteros-Yáñez, A.S. Migallón, S. Merino, E. Vázquez, Magnetically responsive hydrophobic pockets for on–off drug release, Mater. Today Chem. 23 (2022) 100702, https://doi.org/10.1016/j.mtchem.2021.100702.

[33] J. Leganés, A. Sánchez-Migallón, S. Merino, E. Vázquez, Stimuli-responsive graphene-based hydrogel driven by disruption of triazine hydrophobic interactions, Nanoscale 12 (2020) 7072–7081, https://doi.org/10.1039/c9nr10588c.

[34] M.J. Penn, M.G. Hennessy, Optimal loading of hydrogel-based drug-delivery systems. http://arxiv.org/abs/2202.02025, 2022.

[35] J.D. Van Dyke, K.L. Kasperski, Thermogravimetric study of polyacrylamide with evolved gas analysis, J. Polym. Sci. Polym. Chem. 31 (1993) 1807–1823, https://doi.org/10.1002/pola.1993.080310720.

[36] J.M. González-Domínguez, E. Vázquez, R. Rauti, S. Merino, C. Martín, L. Ballerini, M. Prato, Graphene improves the biocompatibility of polyacrylamide hydrogels: 3D polymeric scaffolds for neuronal growth, Sci. Rep. 7 (2017) 10942, https://doi.org/10.1038/s41598-017-11359-x.

[37] T. Qian, J. Li, W. Feng, H. Nian, Enhanced thermal conductivity of form-stable phase change composite with single-walled carbon nanotubes for thermal energy storage, Sci. Rep. 7 (2017), https://doi.org/10.1038/srep44710.

[38] M.F. Gómez-Rico, R. Font, A. Fullana, I. Martín-Gullón, Thermogravimetric study of different sewage sludges and their relationship with the nitrogen content, in: J Anal Appl Pyrolysis, Elsevier, 2005, pp. 421–428, https://doi.org/10.1016/j.jaap.2004.11.029.

[39] G. Stojkov, Z. Niyazov, F. Picchioni, R.K. Bose, Relationship between structure and rheology of hydrogels for various applications, Gels 7 (2021), https://doi.org/10.3390/gels7040255.

[40] J. Zhang, N. Wang, W. Liu, X. Zhao, W. Lu, Intermolecular hydrogen bonding strategy to fabricate mechanically strong hydrogels with high elasticity and fatigue resistance, Soft Matter 9 (2013) 6331, https://doi.org/10.1039/c3sm50866h.

[41] N. Huebsch, J. Kim, X. Zhao, K. Lee, C.A. Cezar, K. Bouhadir, D.J. Mooney, Active scaffolds for on-demand drug and cell delivery, Proc. Natl. Acad. Sci. USA 108 (2010) 67–72, https://doi.org/10.1073/pnas.1007862108.

[42] H. Ramli, N.F.A. Zainal, M. Hess, C.H. Chan, Basic principle and good practices of rheology for polymers for teachers and beginners, Chemistry Teacher International 4 (2022) 307–326, https://doi.org/10.1515/cti-2022-0010.

[43] S. Correa, A.K. Grosskopf, H. Lopez Hernandez, D. Chan, A.C. Yu, L.M. Stapleton, E. A. Appel, Translational applications of hydrogels, Chem Rev 121 (2021) 11385–11457, https://doi.org/10.1021/acs.chemrev.0c01177.

[44] Z. Li, C. Yu, H. Kumar, X. He, Q. Lu, H. Bai, K. Kim, J. Hu, The effect of crosslinking degree of hydrogels on hydrogel adhesion, Gels 8 (2022), https://doi.org/10.3390/gels8100682.

[45] A. Martín-Pacheco, A. Esau, R. Del, C. Martín, M.A. Herrero, S. Merino, J. Luis García Fierro, E. Díez-Barra, E. Vázquez, Graphene quantum dot − aerogel: from nanoscopic to macroscopic fluorescent materials. Sensing polyaromatic compounds in water, ACS Appl. Mater. Interfaces 10 (2018) 18192–18201, https://doi.org/10.1021/acsami.8b02162.

[46] N.S. Vrandečić, M. Erceg, M. Jakić, I. Klarić, Kinetic analysis of thermal degradation of poly(ethylene glycol) and poly(ethylene oxide)s of different molecular weight, Thermochim. Acta 498 (2010) 71–80, https://doi.org/10.1016/j.tca.2009.10.005.

[47] S. Jonathan, The infrared and Raman spectra and structure of acrylamide, J. Mol. Spectrosc. 6 (1961) 205–214.

[48] P. Kumar, C. Joshi, A.K. Srivastava, P. Gupta, R. Boukherroub, S.L. Jain, Visible light assisted photocatalytic [3 + 2] azide-alkyne "click" reaction for the synthesis of 1,4-substituted 1,2,3-triazoles using a novel bimetallic Ru-Mn complex, ACS Sustain Chem Eng 4 (2016) 69–75, https://doi.org/10.1021/acssuschemeng.5b00653.

[49] M.O. Mohsen, M.F. Bachmann, Virus-like particle vaccinology, from bench to bedside, Cell. Mol. Immunol. 19 (2022) 993–1011, https://doi.org/10.1038/s41423-022-00897-8.

[50] A.E. Czapar, B.D.B. Tiu, F.A. Veliz, J.K. Pokorski, N.F. Steinmetz, Slow-release formulation of cowpea mosaic virus for in situ vaccine delivery to treat ovarian cancer, Adv. Sci. 5 (2018), https://doi.org/10.1002/advs.201700991.

[51] A. Staśkiewicz, P. Ledwoń, P. Rovero, A.M. Papini, R. Latajka, Triazole-modified peptidomimetics: an opportunity for drug Discovery and development, Front. Chem. 9 (2021), https://doi.org/10.3389/fchem.2021.674705.

[52] X. Tong, J. Lai, B.H. Guo, Y. Huang, A new end group structure of poly(ethylene glycol) for hydrolysis-resistant biomaterials, J. Polym. Sci. Polym. Chem. 49 (2011) 1513–1516, https://doi.org/10.1002/pola.24562.

[53] X. Huang, C.S. Brazel, On the importance and mechanisms of burst release in matrix-controlled drug delivery systems, J. Contr. Release 73 (2001) 121–136, https://doi.org/10.1016/S0168-3659(01)00248-6.